Available online at www.sciencedirect.com
ScienceDirect
International Journal of Multiphase Flow 32 (2006) 1354–1369
International Journal of Multiphase Flow
www.elsevier.com/locate/ijmulflow

Variation of fiber orientation in turbulent flow inside a planar contraction with different shapes

M. Parsheh [a], M.L. Brown [b], C.K. Aidun [c,*]

[a] Institute of Paper Science and Technology, Georgia Institute of Technology, Atlanta, GA 30332, USA
[b] School of Chemical and Biomolecular Engineering, Georgia Institute of Technology, Atlanta, GA 30332, USA
[c] G.W. Woodruff School of Mechanical Engineering, Georgia Institute of Technology, Atlanta, GA 30332, USA

Received 14 October 2005; received in revised form 9 July 2006

Abstract

In this study, we have investigated the influence of shape of planar contractions on the orientation distribution of stiff fibers suspended in turbulent flow. To do this, we have employed a model for the orientational diffusion coefficient based on the data obtained by high-speed imaging of suspension flow at the centerline of a contraction with flat walls. This orientational diffusion coefficient depends only on the contraction ratio and turbulence intensity. Our measurements show that the turbulence intensity decays exponentially independent of the contraction angle. This implies that the turbulence variation in the contraction is independent of the shape, consistent with the results by the rapid distortion theory and the experimental results of axisymmetric contractions. In order to determine the orientation anisotropy, we have solved a Fokker–Planck type equation governing the orientation distribution of fibers in turbulent flow. Although the turbulence variation and the orientational diffusion are independent of the contraction shape, the results show that the variation of the orientation anisotropy is dependent on shape. This can be explained by the variation of the rotational Péclet number, Pe_r, inside the contractions. This quantity is a measure of the importance of the mean rate of the strain relative to the orientational diffusion. We have shown that when $Pe_r < 10$ turbulence can significantly influence the evolution of the orientation anisotropy. Since in contractions with identical inlet conditions the streamwise position where $Pe_r = 10$ depends on the shape, the orientation anisotropy is dependent on the variation of rate of strain in a given contraction. We demonstrate the shape effect by considering contraction with flat walls as well as three contractions with different mean rate of strain variation.

Keywords: Fiber suspension; Orientational diffusion; Fiber orientation; Orientation distribution function; Turbulent flow; Planar contraction; Rotational Péclet number; High-speed imaging

1. Introduction

Motion and orientation of suspended fibers in turbulent flow affect transport, rheology, and turbulence characteristics of the suspension. In addition, in many industrial processes the quality of the final products

* Corresponding author. Tel.: +1 404 894 6645; fax: +1 404 894 4778.
E-mail address: cyrus.aidun@me.gatech.edu (C.K. Aidun).

0301-9322/$ - see front matter © 2006 Elsevier Ltd. All rights reserved.
doi:10.1016/j.ijmultiphaseflow.2006.07.002

is dependent on the orientation of fibers. For example, in papermaking, mechanical properties of manufactured paper are known to be anisotropic due to the anisotropy in the orientation distribution of fibers induced by the flow kinematics while passing through a planar contraction. One of the primary parameters which can be changed to alter the orientation distribution function in converging flows is the shape of the contraction.

The dynamics and orientation of an inertialess ellipsoid in a linear shear flow can be obtained from Jeffery's equation (1922). The tensorial form of this equation is given by

$$\dot{p}_i = \Omega_{ij} p_j + \lambda(E_{ij} p_j - E_{kl} p_k p_l p_i), \tag{1}$$

where p_i, Ω_{ij} and E_{ij} denote the unit orientation vector along the longitudinal axis of the particle, the antisymmetric and symmetric part of the velocity gradient tensor, respectively; and $\lambda(\equiv [a_p^2 - 1]/[a_p^2 + 1])$ is a function of the fiber aspect ratio, a_p.

Brenner (1974) generalized this approach to cover any axisymmetric particle. This analysis is valid when the suspension is dilute, i.e., each fiber can rotate freely without affecting the motion of other fibers or its motion become affected by other fibers (Bibbo et al., 1985). This requires $n < 1/l^3$, where n and l denote the number of fibers per unit volume and the fiber half length, respectively. When $n > 1/l^3$, fibers hydrodynamically interact and influence their orientation state. Thus, in a semi-dilute suspension the motion of a fiber depends on the mean fluid velocity, the fluctuating component of the fluid velocity, hydrodynamic fiber–fiber interactions, and inertia.

In order to quantify the effect of hydrodynamic fiber–fiber interactions on orientation, Shaqfeh and Koch (1990) developed a model based on kinetic theory to predict the dispersion of fibers oriented along the extensional axis of axisymmetric and planar extensional flows. This model shows that the orientational dispersion for dilute and semi-dilute suspensions is $O(nl^3/\ln^2 a_p)$ and $O(\ln(nl^3)/nl^3)$, respectively. In the dilute regime, as the concentration increases from infinite-dilute, the rate of dispersion increases. While in the semi-dilute regime the dispersion rate decreases with increasing fiber concentration. This decrease at semi-dilute regime is attributed to the short range screening of hydrodynamic disturbances (see e.g., Shaqfeh, 1988; Shaqfeh and Fredrickson, 1990; Shaqfeh and Koch, 1990). Shaqfeh and Koch also observed that the fiber dispersion in a planar extensional flow is anisotropic in the dilute regime. Dispersion in the transverse direction was shown to be larger than that in the direction of extension.

The orientation state of a large number of fibers is described by the probability distribution function, $\psi(\mathbf{p}, t)$. This function is normalized such that

$$\oint \psi(\mathbf{p}, t)\, \mathrm{d}\mathbf{p} = 1 \tag{2}$$

(Dinh and Armstrong, 1984). Based on the conservation principles in the $\mathbf{p}$ space, distribution function must satisfy the continuity equation given by

$$\frac{\mathrm{D}\psi}{\mathrm{D}t} + \nabla_{\mathrm{r}} \cdot (\dot{\mathbf{p}}\psi) = 0, \tag{3}$$

where ∇_{r} is the gradient operator in orientation space (i.e., the gradient operator of the surface of a unit sphere). Analogous to suspension flows with Brownian motion and with hydrodynamic fiber–fiber interactions, the change of orientation distribution function $\psi(\mathbf{p}, t)$ in turbulent flows can be modeled by a Fokker–Planck type equation (see e.g., Advani and Tucker, 1987; Doi and Edwards, 1988; Krushkal and Gallily, 1988; Koch, 1995; Olson and Kerekes, 1998) given by

$$\frac{\mathrm{D}\psi}{\mathrm{D}t} = \nabla_{\mathrm{r}} \cdot (\mathbf{D}_{\mathbf{r}} \cdot \nabla_r \psi - \dot{\mathbf{p}}\psi), \tag{4}$$

where $\mathbf{D}_{\mathbf{r}}$ is the rotational diffusion coefficient tensor. In this equation, the translational diffusion is neglected because the fiber concentration in the suspension flow is assumed to be homogeneous. Depending on the flow conditions, the diffusion term on the right hand side of (4) represents the randomizing effect due to either the Brownian motion (Doi and Edwards, 1988), the turbulent eddies (Krushkal and Gallily, 1988; Olson and Kerekes, 1998) or the hydrodynamic fiber–fiber interactions (Koch, 1995). In this study, we consider that the rotational diffusion is isotropic and thus is represented by a scalar diffusion coefficient, D_{r}, instead of a tensor.

In turbulent flows, the dispersion of fibers is altered due to the presence of velocity fluctuations. Krushkal and Gallily (1988) experimentally studied the development of orientation distribution of non-spherical aerosol particles in a turbulent shear flow. They concluded that particles become randomly oriented in the presence of turbulence with high intensity. However, for flow with mean velocity gradients, the orientation distribution function is anisotropic if the turbulence intensity is not sufficiently large to randomize the particles. Bernstein and Shapiro (1994) investigated the orientation of glass fibers in laminar and turbulent pipe flow. They found that at low Reynolds number laminar flow, the fibers are randomly distributed near the pipe center. As the Reynolds number increases within the laminar regime, the fibers become more oriented in the streamwise direction. At high Reynolds number turbulent flow, the randomizing effect of the turbulence leads to a nearly isotropic orientation.

Olson and Kerekes (1998) expressed the rotational diffusion coefficient in an isotropic turbulent flow as a function of turbulent integral time and length scales, turbulence intensity and fiber length. They found that by increasing the ratio of the fiber length to the Lagrangian integral length scale, the diffusion coefficient decreases. Recently, Shin and Koch (2005) numerically showed that the rotational diffusion coefficient, D_r, is of the order of the inverse integral time scale. In a planar contraction, Olson et al. (2004) numerically solved the Fokker–Planck equation governing the orientation distribution of fibers. Through comparison with measured data, they showed that D_r is constant throughout the contraction. Since in the study by Olson et al. the flow into the contraction passed through a package of tubes with sudden increase in the diameter, the inlet flow to the contraction is different from the present study. Turbulence in contractions is highly dependent on the inlet flow characteristics, therefore, the model by Olson et al. (2004) is expected to be inaccurate for isotropic, homogeneous grid-turbulence flow.

In axisymmetric contractions, it has been shown that the contraction shape and flow Reynolds number do not have considerable influence on the turbulence characteristics. Rather the inlet turbulence condition is the most dominating parameter, as shown by Hussain and Ramjee (1976) and Ramjee and Hussain (1976). Several questions have remained open in planar contractions. Are the turbulence characteristics inside planar contractions independent of the contraction shape as well? How does the rotational diffusion coefficient, D_r, vary inside contractions? Does the production of turbulent kinetic energy inside contractions influence D_r? Is the orientation distribution function dependent on contraction shape? The objective of this study is to investigate whether the orientation anisotropy and turbulence characteristics inside contractions are affected by contraction shape. To do this, we solve a Fokker–Planck type equation with an isotropic rotational diffusion coefficient, D_r. Thus, we need a relation for D_r in contractions. This is accomplished by using a model developed by Parsheh et al. (2005) based on the measured orientation distribution function at the centerline of a planar contraction with flat walls (see Fig. 1). We study the effect of contractions on isotropic homogeneous turbulence while changing the contraction angle in order to examine the influence of the contraction shape on turbulence, as outlined in Brown et al. (2006). To investigate the influence of turbulence on the orientation anisotropy, we have designed the experiments such that the measured results are not influenced

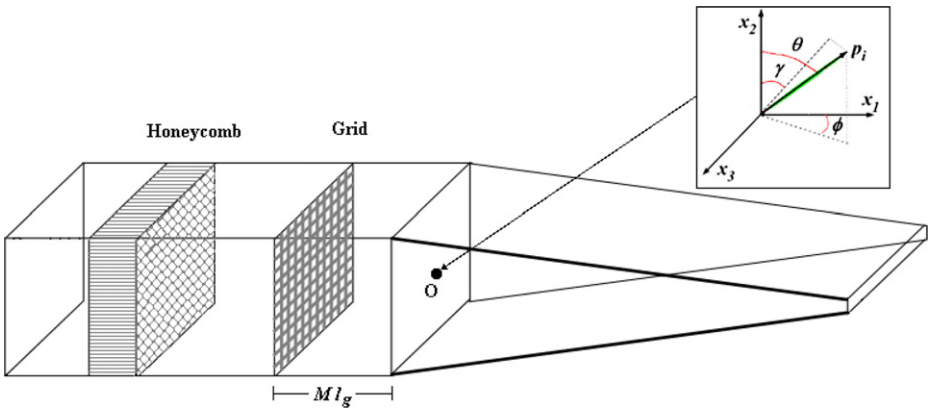

Fig. 1. Schematic of the experimental set-up with coordinate system.

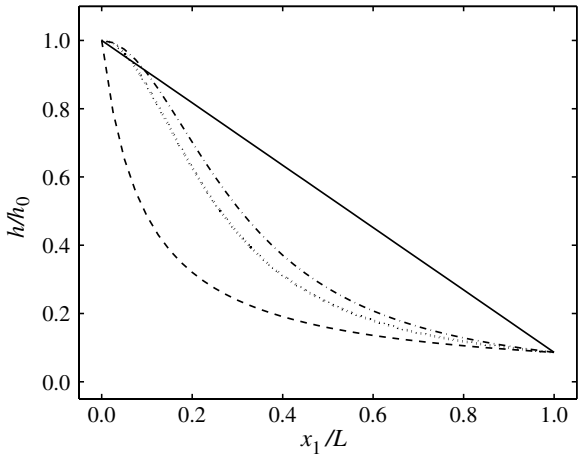

Fig. 2. Contraction geometries considered; flat plate Eq. (8) (—), constant rate of strain Eq. (5) (- - -), linear rate of strain Eq. (6) (–·–), quadratic rate of strain Eq. (7) (· · ·).

by the hydrodynamic fiber–fiber interactions and the fibers do not affect the flow field (Paschkewitz et al., 2005). A nearly isotropic homogeneous grid-turbulence is introduced at the contraction inlet. In order to obtain reliable average data, the motion and orientation of a large population of fibers are measured. The results of these measurements are presented as the development of the orientation distribution function at different downstream positions.

We have investigated the influence of contraction shape on orientation anisotropy by analyzing the orientation distribution function in contractions with constant mean rate of strain, linear rate of strain, quadratic rate of strain and flat walls. The equation of local height for these contractions is given by

$$h = \frac{h_0 L}{(C_{\max} - 1)x_1 + L}, \tag{5}$$

$$h = \frac{h_0 L^2}{(C_{\max} - 1)x_1^2 + L^2}, \tag{6}$$

$$h = \frac{2h_0 L^3}{3(C_{\max} - 1)L x_1^2 - (C_{\max} - 1)x_1^3 + 2L^3}, \tag{7}$$

and

$$h = h_0 - 2x_1 \tan\beta, \tag{8}$$

respectively, where h_0, $C_{\max}$, L, and Q denote the inlet contraction height, the maximum contraction ratio, contraction length and flow rate per unit width, respectively. The contraction ratio is defined as

$$C = \frac{U_1}{U_{1,0}}, \tag{9}$$

where U_1 and $U_{1,0}$ denote the local streamwise mean velocity and the streamwise mean inlet velocity, respectively. Fig. 2 shows the schematic of these contraction shapes.

2. Experimental set-up

In an earlier study (Parsheh et al., 2005), we have reported visualization of stiff fibers suspended in turbulent flow at the centerline of a planar contraction with flat walls, Fig. 1. Based on these data, we investigated evolution of fiber orientation distribution in the contraction and derived a model for the rotational Péclet number, Pe_r. This model is dependent only on contraction ratio and inlet turbulence conditions, independent of the production of turbulent kinetic energy in the contraction. In the present study, we employ this model to

investigate the contraction shape effect. Also, we have investigated the evolution of turbulence at the centerline of contractions with flat walls (Parsheh et al., 2005; Brown et al., 2006). The flow facility, velocity field and fiber orientation measurement methods are briefly outlined below.

2.1. Flow facility and velocity measurements

Orientation of fibers suspended in turbulent flow inside a small closed water loop is measured using high-speed imaging, Parsheh et al. (2005). The test section is constructed from 12 mm-thick Plexiglas to allow for visual access. Flow first passes through a hexagonal flow straightener installed in a constant cross-section channel upstream of the contraction. The flow straightener has an open width of 10 mm and a closed width of 0.4 mm. Free-stream turbulence is then generated by a monoplane square grid with rectangular bars. The mesh size, M, and bar width of the grid are 9.5 mm, and 3.2 mm respectively, resulting in a solidity of 0.56 (solidity is defined as the grid geometric blockage area divided by the total area). The distance between the grid and the contraction inlet is normalized by mesh size, M, and is denoted by l_g hereafter. The origin of the coordinate system is located at the contraction inlet and the streamwise direction is denoted by x_1, see Fig. 1. The contraction is 550 mm in length, 155 mm wide, inlet height is 179.2 mm, and the outlet height is 16 mm giving the contraction half angle, $\beta = 8.4°$, and maximum contraction ratio, $C_{max} = 11.2$. The flow Reynolds number is defined as

$$Re = \frac{U_1 h}{v}, \tag{10}$$

where h and v denote the contraction height and the fluid kinematic viscosity, respectively. This parameter remains constant throughout the contraction. In these experiments, Re is 85×10^3 with exit velocity 4.9 m/s. The estimated average streamwise velocity component based on irrotational flow assumption is given by

$$U_1 = \frac{Q}{h_0 - 2x_1 \tan\beta}, \tag{11}$$

where Q and h_0 denote the flow rate per unit width and the inlet height, respectively.

A two component laser-Doppler anemometry (TSI) with a 5 W argon ion laser (Coherent, Innova 70) is used to measure the velocity field. Alumina particles, 0.3 μm in diameter, are used to seed the flow. The optical head is traversed automatically using a three-dimensional linear traversing system with accuracy of ±0.1 mm. The LDA data are collected randomly with five repetitions for a period of 90 s.

2.2. Visualization and image processing technique

In Parsheh et al. (2005) a dilute suspension of stiff opaque rayon fibers is visualized. The fibers are nominally 3.2 mm in length, 57 μm in diameter, with specific gravity equal to 1.14. The suspension's nl^3 is 0.0053. We have dried the fibers in an oven at 105 °C for 24 h or more.

Motion of suspended fibers in the x_1–x_3 plane is visualized using a pulsed laser sheet and a high-speed camera. A pulsed infra-red laser sheet at wavelength 808 nm (Oxford model HSI1000) with pulse duration of 15 μs is synchronized with a V5 Phantom high-speed camera. A lens is used to project a 3.2 mm thick, 100 mm wide laser sheet into the contraction. The laser head is translated linearly in the x_2-direction with a resolution of 0.01 mm. The camera is translated linearly in the x_1, x_2 and x_3 directions and rotates around x_3-axis. Images are taken at the centerplane of the contraction, defined as the x_1–x_3 plane located within $x_2 = \pm 1.6$ mm. They have a dimension of 9.6 mm in the x_1-direction and 14.5 mm in the x_3-direction with 342×512 pixel resolution. We have analyzed 8190 images at each position which the resulted orientation distribution function, ψ, is evaluated from a succession of approximately 4000 randomly imaged fibers.

Softwares are developed which inverts the image, scans the frame, and identifies each fiber in the image. The fibers are rigid but they are not all perfectly straight. Thus, to accurately evaluate the orientation of an observed fiber, we divide the fiber into 5 or more equal segments. A line is then fitted to each segment, and

the angle of the segments of each fiber are averaged and used to determine the fiber orientation distribution. A complete description of the image analysis technique is given in Parsheh et al. (2005).

Throughout this paper, the orientation anisotropy parameter will be presented versus contraction ratio. However, the contraction ratio, C, varies slightly along the streamwise length of the images, Δx_1. The average contraction ratio, C_a, in each image is given by

$$C_a = \frac{1}{\Delta x_1}\int_{x_{1,1}}^{x_{1,2}} C(x_1)\,dx_1, \tag{12}$$

where $\Delta x_1 = 9.6$ mm and $x_{1,1}$ and $x_{1,2}$ are the upstream and downstream edge positions of the image, respectively. The straight channel upstream of the contraction inlet and the contraction are joined by a set of opaque flanges 30 mm in length. Due to these flanges and the finite length of our images, the first position downstream of the contraction inlet is located at $C_a = 1.1$. In this study, the experimental results are presented versus C_a and from this point on we drop the subscript 'a' for convenience.

3. Development of isotropic homogeneous turbulence in planar contractions

In this section, we discuss the influence of the contraction on the isotropic, homogeneous grid-turbulence at inlet. In order to quantify the impact of turbulence on the orientation distribution, we have introduced grid-turbulence with different intensity into the contraction. This is done by changing the position of the grid relative to the inlet. Cases with grid positions at $l_g = 20$ and $l_g = 60$, where l_g is defined as the number of grid mesh size, are studied. In $l_g = 20$, the inlet turbulence intensity is almost twice as in $l_g = 60$.

In general, grid-generated turbulence tends to have slightly higher energy content in the streamwise direction. Comte-Bellot and Corrsin (1966) used an axisymmetric contraction with $C_{max} = 1.27$ to suppress the streamwise fluctuating velocity component to obtain a perfect isotropic grid-turbulence, where C_{max} denotes the contraction ratio at the outlet. In our measurements, the grid-turbulence at the inlet is nearly isotropic since the difference between the fluctuating velocity components are within $\pm 5\%$. In addition, the spatial variation in the fluctuating velocity components is within $\pm 7\%$ implying a nearly homogeneous turbulence.

The streamwise mean velocity profile along the x_2-axis at $x_3 = 0$, Fig. 3(a), and along the x_3-axis at $x_2 = 0$, Fig. 3(b), is uniform implying that $\partial U_1/\partial x_2 \approx 0$ and $\partial U_1/\partial x_3 \approx 0$ in the core region. Also, the mean velocity in the x_3-direction, U_3, is zero. Based on these facts, the mean velocity gradient tensor at the core region is given by

$$\frac{\partial U_i}{\partial x_j} = \begin{pmatrix} \frac{\partial U_1}{\partial x_1} & \frac{\partial U_1}{\partial x_2} \approx 0 & \frac{\partial U_1}{\partial x_3} \approx 0 \\ \frac{\partial U_2}{\partial x_1} & -\frac{\partial U_1}{\partial x_1} & 0 \\ 0 & 0 & 0 \end{pmatrix}. \tag{13}$$

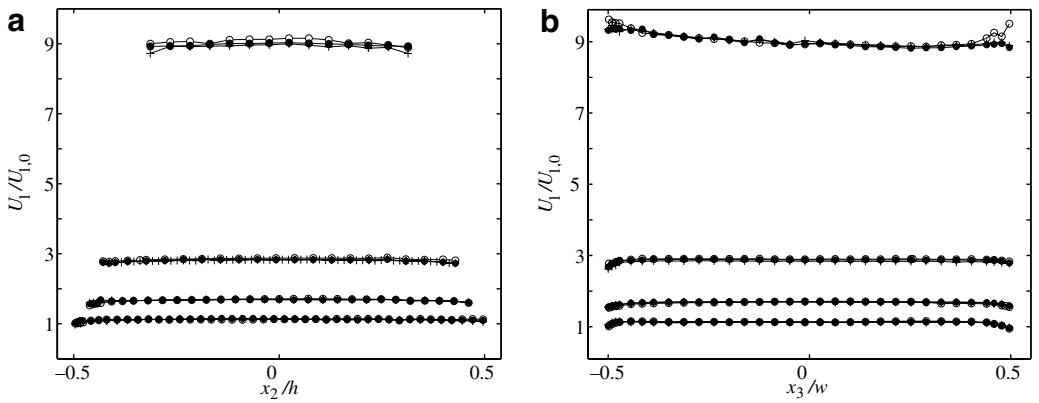

Fig. 3. Mean streamwise velocity profile (a) along the x_2-axis at $x_3 = 0$; (b) along the x_3-axis at $x_2 = 0$ at $C = 1.2$, 1.6, 2.8 and 9.0 (bottom to top) for $Re = 85 \times 10^3$ (○), $Re = 127 \times 10^3$ (●) and $Re = 170 \times 10^3$ (+).

The only non-zero component of mean vorticity vector, which is responsible for the production of turbulence, is given by

$$\omega_3 = \frac{\partial U_2}{\partial x_1}. \tag{14}$$

However, at the contraction centerline this component is zero due to symmetry.

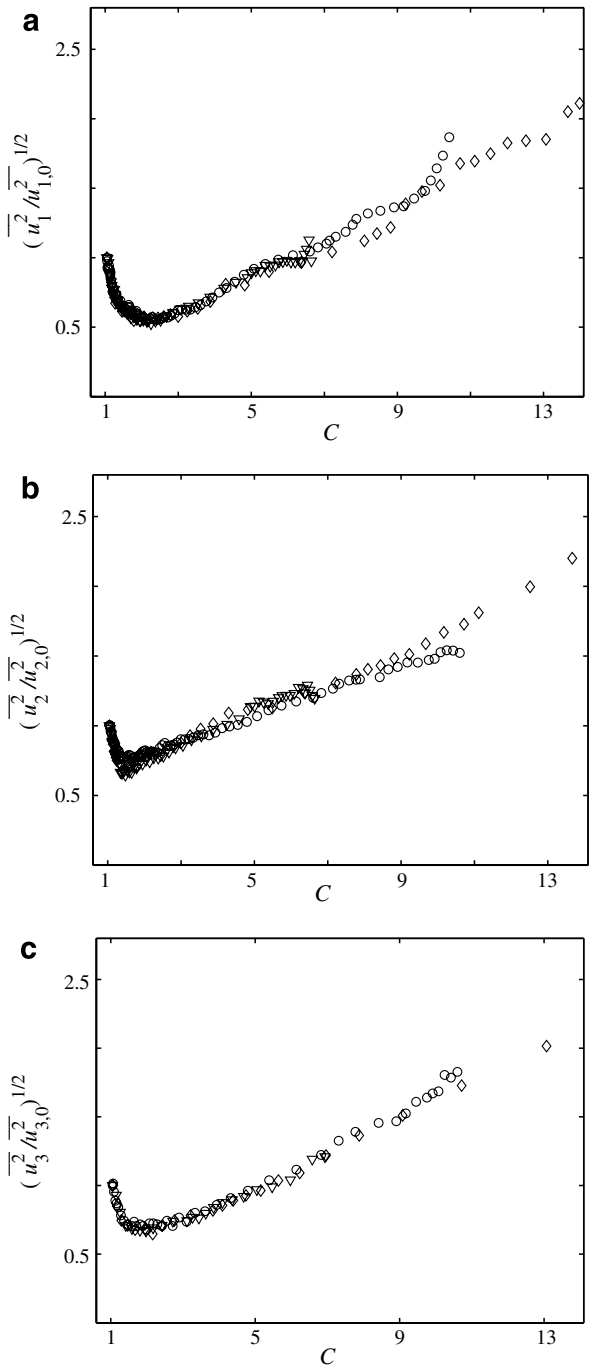

Fig. 4. Effect of contraction angle on (a) x_1-component, (b) x_2-component and (c) x_3-component of the fluctuating velocity for $\beta = 8.15°$ (△), $\beta = 8.4°$ (○) and $\beta = 8.8°$ (◇).

The flow in the core region is not affected by the wall boundaries. Thus, the mean velocity components are in good agreement with the velocity components based on a simple quasi-one-dimensional potential flow, Parsheh et al. (2005).

The fluctuating velocity components attain minimum values inside the contraction, Fig. 4. The minimum in x_1, x_2 and x_3 components in case $l_g = 20$ occur at $C \approx 2.1$, $C \approx 1.7$ and $C \approx 1.8$, respectively. Our measurements show that the position of the minimum is not dependent on the Reynolds number and the contraction angle. However, the minimum in the x_1-component moves from $C \approx 2.1$ to $C \approx 1.7$ when $l_g = 60$ (it is not shown here). This suggests that the turbulence characteristics in the contraction is highly dependent on the inlet flow condition, consistent with the results for axisymmetric contractions by Hussain and Ramjee (1976).

The rapid distortion theory (Ribner and Tucker, 1953; Batchelor and Proudman, 1954) predicts that the variation of the fluctuating velocity components is not influenced by the shape of the contraction. Hussain and Ramjee (1976) verified this matter for axisymmetric contractions by measuring the turbulence in four different axisymmetric contractions. They showed that all contractions affect the core flow similarly and the total acceleration is the primary parameter concerning the evolution of the turbulence. In the present study, we investigate the effect of shape in planar contractions by analyzing the influence of contraction angle, β, on turbulence. This is done by varying the outlet height and keeping other parameters unchanged. Fig. 4(a)–(c) show the fluctuating velocity components in the contractions with maximum contraction ratio of $C_{max} = 7.3$, $C_{max} = 11.2$ and $C_{max} = 16.7$, where the corresponding contraction half-angles are $\beta = 8.15°$, $\beta = 8.4°$ and $\beta = 8.8°$, respectively. Although the difference in angle, β, appears to be small, the total convective acceleration at the contraction outlet when $\beta = 8.8°$ is more than two times larger than that when $\beta = 8.15°$. As shown in Fig. 4(a)–(c) the fluctuating velocity components collapse around the same curve implying that the variation of turbulence characteristics with C is almost independent of β. Based on the results for axisymmetric and planar contractions, it is reasonable to make the assumption that the contraction shape does not have a considerable effect the turbulence characteristics.

The streamwise turbulence intensity component along the centerline, $T_1 = (\overline{u_1^2})^{1/2}/U_1$, decreases monotonically downstream of the inlet to less than 1.5% at the outlet in all cases. This implies that the effect of the turbulence on orientation anisotropy is very small at high contraction ratios. Parsheh et al. (2005) showed that the turbulence intensity in various cases with different Reynolds number, contraction half angle, and inlet turbulence intensity collapse around an exponentially decaying curve. A thorough investigation of the evolution of turbulence in planar contractions is given in Brown et al. (2006).

4. Analysis and results

In this section, we study the orientation distribution of fibers in presence of turbulence as well as when $D_r = 0$ (D_r is the rotational diffusion coefficient). We use then the model for the rotational diffusion coefficient derived by Parsheh et al. (2005). Furthermore, we use the measured orientation distribution as the initial profile for computation of orientation state for inertialess fiber suspension flow with $D_r = 0$ and compare these results to the measured data to determine the impact of turbulence on the orientation anisotropy.

Measured orientation distribution function, ψ, at contraction inlet is not fully isotropic. This is attributed to a slight contraction of flow in the straight channel downstream of the grid due to the boundary layer growth. This slight anisotropy at the contraction inlet is more pronounced for the case with $l_g = 60$. Samples of the measured orientation distribution function when $l_g = 20$ is shown in Fig. 5. According to this figure, more fibers are oriented in the streamwise direction at larger C. Although direct comparison of distribution function can give qualitative differences, as in Fig. 5, we need a method to accurately represent ψ while readily quantifying the downstream development of the orientation distribution function by a numerical index. Advani and Tucker (1987) showed that even-order tensors give a concise description of ψ. The second and fourth order planar orientation tensors in the x_1–x_3 plane are defined as

$$a_{ij} = \int_0^\pi \psi(\phi) p_i p_j \, \mathrm{d}\phi, \tag{15}$$

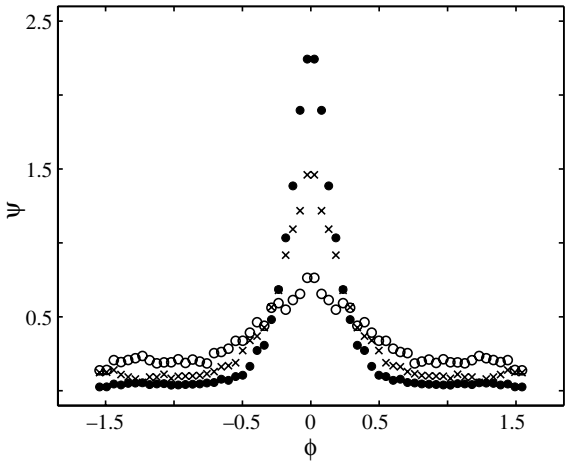

Fig. 5. Orientation distribution function, ψ at $C = 2.3$ (○), $C = 4.8$ (×), and $C = 9.3$ (●) when $Re = 85 \times 10^3$ and $l_g = 60$.

and

$$a_{ijkl} = \int_0^{\pi} \psi(\phi) p_i p_j p_k p_l \, \mathrm{d}\phi, \tag{16}$$

respectively. These symmetric tensors represent moments of the orientation distribution function. The diagonal components of orientation tensor show the degree of alignment and the off-diagonal terms represent the skewness. It has been shown that higher order tensors give a more accurate representation of ψ (Advani and Tucker, 1987). Also, orientation distribution function can be reproduced given the orientation tensor components. In this study, we use one of the normal components of the fourth order planar orientation tensor, a_{1111}, to represent the orientation distribution function. The value of this component varies between 0 and 1.0 when all fibers are oriented in the x_3- and x_1-direction, respectively. For a random distribution of fibers, this value is 0.375.

4.1. The equations governing fiber orientation

Orientation of a single fiber can be characterized by the angles (ϕ, θ) defined in Fig. 1. Goldsmith and Mason (1967) derived the general equations for the time rate of change of orientation angles, $\mathrm{d}\phi/\mathrm{d}t$ and $\mathrm{d}\theta/\mathrm{d}t$, in three-dimensional flows. For large aspect ratio fibers, $\lambda \approx 1$, in the absence of turbulence at the centerplane of planar contractions, where $\partial U_2/\partial x_1 \approx 0$, Olson (2002) showed that

$$\frac{\mathrm{d}\phi}{\mathrm{d}t} = -\frac{1}{2}\left(\frac{\partial U_1}{\partial x_1}\right)\sin(2\phi). \tag{17}$$

Also, based on Jeffery (1922) and Goldsmith and Mason (1967) we can show that for this flow $\mathrm{d}\theta/\mathrm{d}t$ is given by

$$\frac{\mathrm{d}\theta}{\mathrm{d}t} = \frac{1}{4}\left(\frac{\partial U_1}{\partial x_1}\right)\cos(2\phi)\sin(2\theta) + \frac{3}{4}\left(\frac{\partial U_1}{\partial x_1}\right)\sin(2\theta). \tag{18}$$

In these equations, U_1 and $\partial U_1/\partial x_1$ are based on the values at the center of the fiber and are assumed to be constant along the fiber. As Eqs. (17) and (18) imply, fibers rotate toward the stable steady state solution, $\phi = 0°$ and $\theta = 90°$, with angular velocity components $\mathrm{d}\theta/\mathrm{d}t \geqslant \mathrm{d}\phi/\mathrm{d}t$. However, $\mathrm{d}\phi/\mathrm{d}t$ or $\mathrm{d}\theta/\mathrm{d}t$ is zero when the initial fiber angle, $\phi_0 = 90°$ or $\theta_0 = 0°$, respectively. Solution of Eq. (17) is given by

$$\tan\phi = \mathrm{e}^{-\kappa}\tan\phi_0 = \frac{C_0}{C}\tan\phi_0, \tag{19}$$

where

$$\kappa = \int_{x_{1,0}}^{x_1} \frac{1}{U_1}\left(\frac{\partial U_1}{\partial x_1}\right) \mathrm{d}x_1 = \ln\frac{C}{C_0}. \tag{20}$$

The subscript '0' denotes the initial condition and κ is the total dimensionless acceleration imposed on the flow from $x_{1,0}$ to x_1 or C_0 to C. In the absence of turbulence, Eq. (19) relates the planar development of the orientation angle of a single fiber to the flow acceleration in the contraction. Also, the solution of Eq. (18) is given by

$$\tan\theta = \mathrm{e}^{\gamma}\tan\theta_0, \tag{21}$$

where

$$\gamma = \int_{C_{1,0}}^{C_1} \frac{1}{C}\left(\frac{2C^2+\tan^2\phi_0}{C^2+\tan^2\phi_0}\right)\mathrm{d}C. \tag{22}$$

4.2. Effect of turbulence on fiber orientation

From (17) and (4) the planar orientation distribution function in turbulent flow, is given by

$$\frac{\partial\psi}{\partial x_1^*} = \frac{\partial^2\psi}{\partial\phi^2} + Pe_{\mathrm{r}}\frac{\partial}{\partial\phi}\left(\frac{1}{2}\psi\sin(2\phi)\right), \tag{23}$$

where $x_1^*(\equiv x_1/[U_1/D_{\mathrm{r}}])$ is the dimensionless streamwise axis and Pe_{r} is the rotational Péclet number given by

$$Pe_{\mathrm{r}} = \frac{\partial U_1/\partial x_1}{D_{\mathrm{r}}}, \tag{24}$$

as shown by Krushkal and Gallily (1988). Eq. (23) clearly shows that the relevant parameter governing the orientation of fibers is the rotational Péclet number. Thus, the planar orientation distribution function, ψ, can be accurately estimated based on (23) with an appropriate model for Pe_{r}. Parsheh et al. (2005) derived a model for Pe_{r} based on the model by Olson and Kerekes (1998). These authors statistically analyzed the equation of motion of a single fiber suspended in isotropic turbulent flow and derived a relation for the turbulence-induced D_{r}. They suggest that for long fibers, where the Lagrangian particle velocity correlation is the same as the fluid Eulerian velocity correlation (Olson and Kerekes, 1998), D_{r} is dependent on turbulence intensity, Eulerian integral length and time scales. Our measurements show that turbulence intensity decays exponentially with C (Brown et al., 2006). Thus, we conclude that D_{r} varies exponentially inside the contractions. The integral length scale at inlet, Λ_0, is approximately equal to fiber length, $2l$, and remains at the same order of magnitude everywhere in the contraction independent of the Reynolds number (Fig. 6). Based on Olson and Kerekes (1998) and the flow conditions in the contraction, Parsheh et al. (2005) showed that when the fiber length is the same order of the integral length scale, the relation

$$Pe_{\mathrm{r}} = \frac{2l}{T_{1,0}}\frac{\mathrm{d}C}{\mathrm{d}x_1}\mathrm{e}^{0.95C}, \tag{25}$$

gives the best fit between the computed orientation parameter, a_{1111}, and the measured a_{1111} (Fig. 7). Also, based on this model, estimated orientation distribution is in good agreement with the measured data (Fig. 8). We have used measured value of ϕ at $C = 1.1$ as the initial angle, ϕ_0, in Eq. (17) to obtain the downstream orientation distribution when $D_{\mathrm{r}} = 0$. The effect of turbulence on the orientation can be clearly observed by comparing computed ψ when $D_{\mathrm{r}} = 0$ with the measured ψ, as shown in Fig. 7. Using the initial distribution at $C = 1.1$ with $l_{\mathrm{g}} = 60$, we have included the model by Olson et al. (2004), i.e., $D_{\mathrm{r}} = 2\ \mathrm{s}^{-1}$. The deviation in results between the model by Olson et al. (2004) and our data is partly due to the difference in inlet turbulent conditions.

Parsheh et al. (2005) showed that the influence of turbulence on the orientation state vanishes at roughly $Pe_{\mathrm{r}} > 10$. Since the rotational Péclet number is the ratio of the mean rate of strain to D_{r}, the orientation state

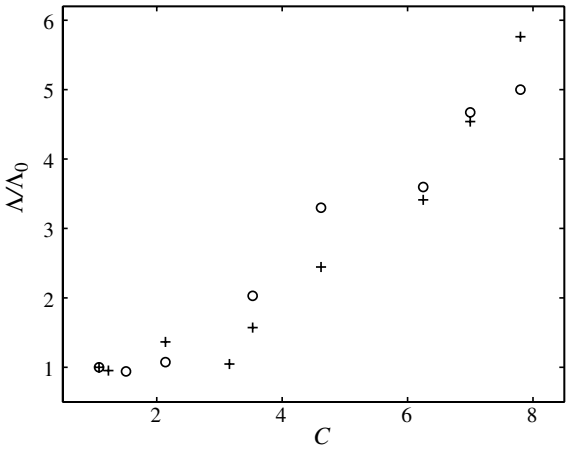

Fig. 6. Eulerian integral length scale when $l_g = 20$ and $Re = 85 \times 10^3$ (+), $Re = 175 \times 10^3$ (○).

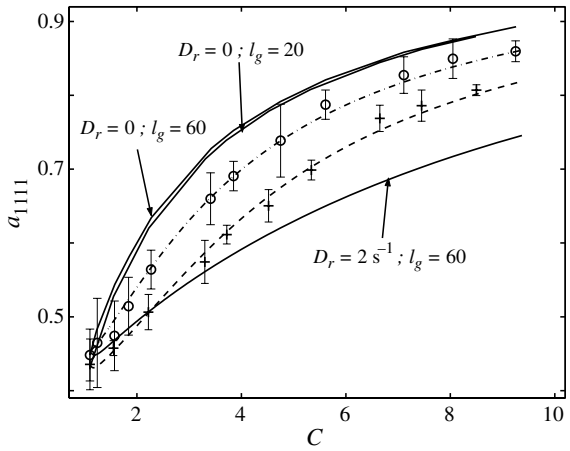

Fig. 7. Variation of a_{1111} when $l_g = 60$: measured (○), computed based on our model Eq. (25) (–·–); $l_g = 20$: measured (+), computed based on our model Eq. (25) (---). Error bars represent 95% confidence intervals.

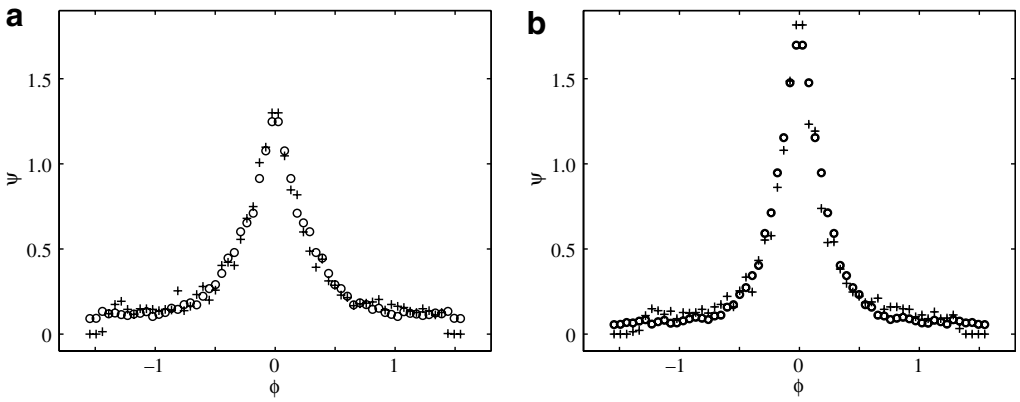

Fig. 8. Orientation distribution function: measured when $l_g = 60$ (○) and computated based on our model given by (25) (+); (a) at $C = 3.4$, (b) at $C = 5.6$, measured orientation at $C = 1.1$ in case $l_g = 60$ is used as the initial value of computation.

can be different in different contraction shapes for identical D_r, as discussed with more detail in the next section.

For large C the microscopic Reynolds number based on the fiber half length, defined as $Re_f = (\partial U_1/\partial x_1)l^2/\nu$, reaches values of the order of 10^2. Despite this large microscopic Reynolds number, inertia has a negligible effect on fiber motion since fiber orientation follows Eq. (17) at large C. Aidun et al. (1998) and Ding and Aidun (2000) showed that at moderate microscopic Reynolds number, the motion of an ellipsoid follows Jeffery's orbit with a slight time delay which accumulates over several orbits. For small angle of rotation, the deviation is very small. The effect of inertia becomes clear after a few orbits where there is a noticeable deviation from Jeffery's solution. Therefore, we conclude that for the relatively small angle of rotation in these experiments, ($<\pi/2$), the effect of inertia is negligible in the sense that it cannot be measured.

4.3. Effect of contraction shape on fiber orientation

We previously showed that production of turbulent kinetic energy has a negligible effect on the variation of turbulence characteristics inside the contraction, and the inlet turbulence condition determines the turbulence level and orientation anisotropy. Therefore, the rotational diffusion coefficient, D_r, is dependent only on the inlet flow conditions. Based on these facts, we examine the effect of contraction shape on fiber orientation anisotropy. We investigate the change of orientation anisotropy in four contraction shapes, characterized by constant mean rate of strain, linear rate of strain, quadratic rate of strain and the planar contraction with flat walls, are outlined in Eqs. (5)–(8). The inlet height, h_0, the contraction length, L, and the maximum contraction ratio, C_{max}, are kept equal in all cases (see Fig. 2). We have used our model given by Eq. (25) to evaluate D_r based on inlet flow conditions in case $l_g = 20$. Therefore, the value of D_r and κ are independent of contraction shape (See Eqs. 20 and 25). The evolution of the rotational Péclet number for these contractions is shown in Fig. 9.

We have solved Eq. (23) for the flow at the contraction centerline using finite difference approximation with isotropic inlet orientation condition. The orientation parameter, a_{1111}, versus the contraction length and the contraction ratio, C, is shown in Figs. 10 and 11, respectively. The contraction with flat walls, which is widely used in industrial processes, has the smallest orientation anisotropy at the outlet. However, the contraction with constant rate of strain gives the largest outlet anisotropy. This is attributed to the interaction of turbulence and mean rate of strain at the region immediately downstream of the inlet. To show the actual comparison of the orientation anisotropy in these cases, the orientation distribution function of the contraction with constant rate of strain and flat walls at $C = 11.2$ are presented in Fig. 12. At roughly $C > 4$, the randomizing effect of turbulence is negligible compared to the orienting effect of the convective flow acceleration. Therefore, in this region a_{1111} develops similarly in all contractions and the orientation anisotropy follows the development with $D_r = 0$, as shown in Fig. 11. The initial rate of strain plays a significant role at $C < 4$ where D_r is

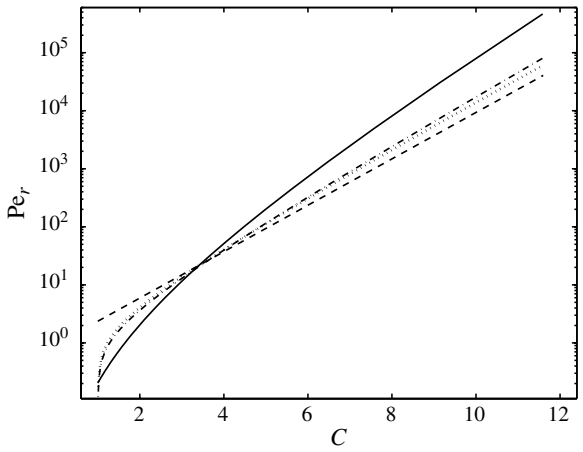

Fig. 9. The rotational Péclet number for flat plate (—), constant rate of strain (---), linear rate of strain (–·–), quadratic rate of strain (···).

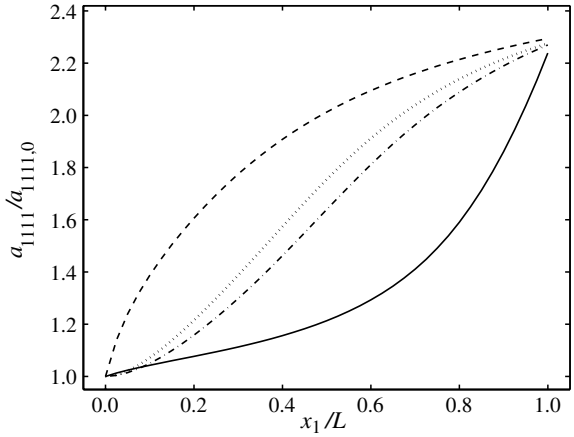

Fig. 10. Variation of a_{1111} with contraction length in case: flat walls, Eq. (8), (—); constant rate of strain, Eq. (5), (---); linear rate of strain, Eq. (6), (–·–); and quadratic rate of strain, Eq. (7), (···).

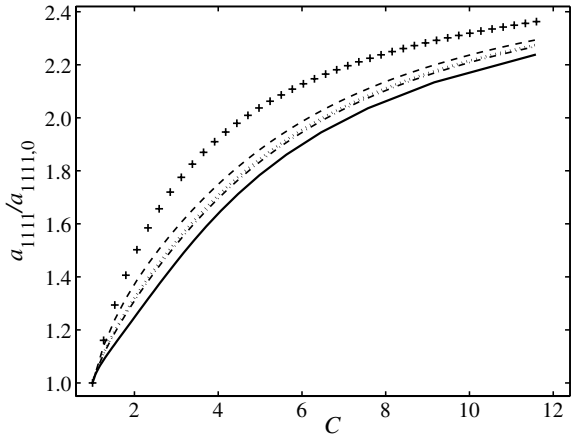

Fig. 11. Variation of a_{1111} with C in case: flat walls, (—), constant rate of strain (---), linear rate of strain (–·–), quadratic rate of strain (···), and when $D_r = 0$ (+).

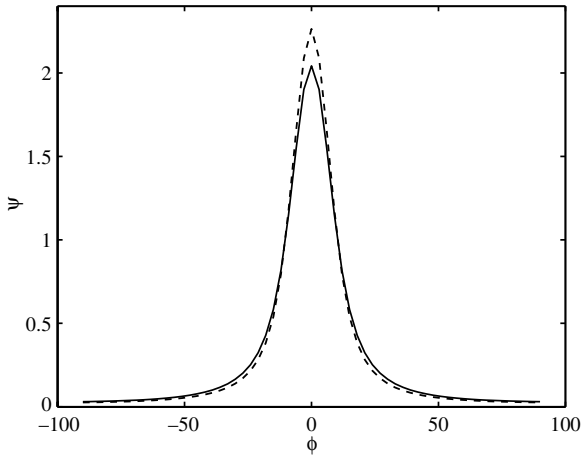

Fig. 12. The orientation distribution function at $C = 11.2$ in case flat walls (—), and constant rate of strain (---).

large. In the cases considered here, in those contractions with larger initial rate of strain at $C < 4$, the randomizing effect of turbulence is effectively overcome by the converging mean flow. Thus, the orientation anisotropy is largest in the case with constant rate of strain. In the channel with flat walls, which has a small initial mean rate of strain, turbulence has a significant randomization effect at $C < 4$.

We have shown that rotational Péclet number is an effective parameter to evaluate the effect of turbulence on fiber orientation anisotropy. Also, this parameter more effectively explains the shape effect. A closer look at Pe_r for the contractions considered in this study (Fig. 9) clearly shows that turbulence has a negligible effect on orientation anisotropy when $Pe_r > 10$, consistent with what we have observed for the measured cases. The cases with smaller Pe_r at $C < 4$ have smaller orientation anisotropy at the outlet, as shown in Fig. 9.

It should be noted that in inertialess suspension flow with $D_r = 0$, a_{1111} is only a function of C and, therefore, is independent of contraction shape. This is attributed to the fact that the change of orientation angle in inertialess suspension flow with $D_r = 0$ is only dependent on the dimensionless acceleration, κ given by Eq. (20). The value of κ is identical in all contractions for a given contraction ratio (see Eqs. (19) and (20)).

The ratio of a_{1111} at $C = 11.2$ for contractions with constant rate of strain, $a_{1111,c}$, and flat walls, $a_{1111,f}$, is shown in Fig. 13. In this figure, the dimensionless rotational diffusion coefficient, D_r^*, is defined as

$$D_r^* = \frac{D_r(x_1 = 0)}{U_{1,0}} 2l. \tag{26}$$

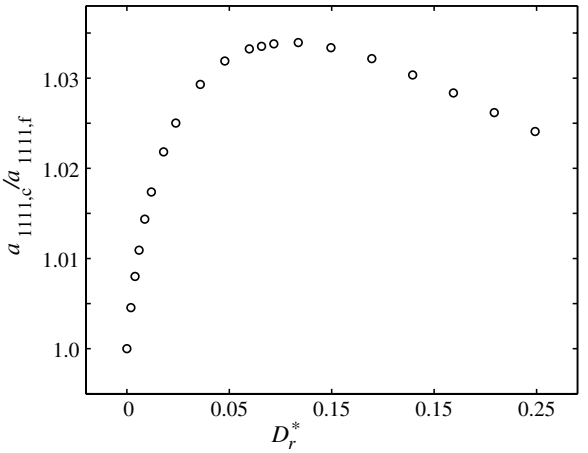

Fig. 13. The ratio of orientation parameter in the case constant rate of strain, $a_{1111,c}$, to the case flat walls, $a_{1111,f}$, at $C = 11.2$.

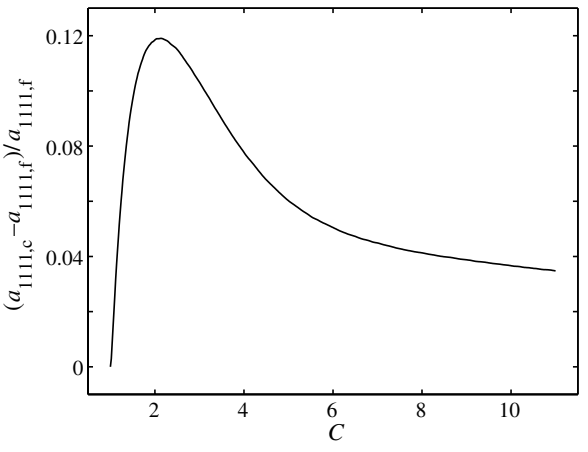

Fig. 14. The streamwise evolution of difference in orientation anisotropy in constant rate of strain contraction and in flat walls when $D_r^* = 0.085$.

When $D_r^* = 0$, fiber orientation is independent of the contraction shape (see Eq. (19)) and for highly turbulent flow when D_r^* is very large, the orientation distribution approaches isotropic state independent of contraction shape. As a result, in both cases $a_{1111,c}/a_{1111,f}$ is equal to one. The value of D_r^* for the cases where $l_g = 20$ and $l_g = 60$ are 0.022 and 0.015, respectively. As Fig. 13 shows, when $D_r^* \approx 0.085$, $a_{1111,c}/a_{1111,f}$ reaches its peak suggesting that the largest effect of the contraction shape on orientation anisotropy in contractions with flat walls and constant rate of strain occurs when $D_r^* \approx 0.085$. A closer look at the difference in $a_{1111,c}$ and $a_{1111,f}$ when $D_r^* = 0.085$ in Fig. 14, reveals that the peak occurs at $C \approx 2.2$ where the shape effect is largest. This figure clearly shows that $a_{1111,c}$ and $a_{1111,f}$ develop differently inside the two contractions. This example clearly shows that the orientation distribution function is a function of contraction shape.

5. Conclusions

The microstructure of fiber suspensions is known to depend on flow kinematics. The flow induced change in microstructure directly impacts the product quality in many industrial applications. We have predicted orientation distribution of a dilute fiber suspension flow inside arbitrary contraction shapes for Reynolds number of $O(10^5)$ in the presence of turbulence. This analysis is based on the solution of a Fokker–Planck type equation, which is previously used to model suspension flows with fiber–fiber interaction and Brownian motion. To solve this equation, a relation for turbulence-induced rotational diffusion coefficient, D_r, is required. The model based on the measured fiber orientation distribution in a contraction with flat walls, given by Parsheh et al. (2005), is thus employed to investigate the shape effect in contractions with various shapes.

Although turbulence intensity and rotational diffusion coefficient are independent of the contraction shape, orientation anisotropy parameter, a_{1111}, obtained by evaluating the moments of the orientation distribution function is shown to vary with the contraction shape. We have shown that fiber orientation anisotropy at the outlet is largest for contractions with high initial rate of strain. The development of the orientation anisotropy is governed by the rotational Péclet number, Pe_r, representing the interplay between the randomizing effect of turbulence and the orienting effect of streamwise mean rate of strain. For contraction ratios $C > 4$ where Pe_r is large, turbulence has negligible effect on fiber orientation distribution. Therefore, the orientation anisotropy parameter, a_{1111}, can be predicted based on Jeffery's solution for inertialess suspension flow with $D_r = 0$. In contractions in which rotational Péclet number at $C < 4$ is less than 10, turbulence strongly influences fiber orientation. Therefore, orientation anisotropy is smaller for contractions with small initial rate of strain which gives a small Pe_r at $C < 4$.

References

Advani, S., Tucker, C.J., 1987. The use of tensors to describe and predict fibre orientation in short fiber composites. J. Rheology 31, 751–784.

Aidun, C.K., Lu, Y., Ding, E.J., 1998. Direct analysis of particulate suspensions with inertia using the discrete Boltzmann equation. J. Fluid Mech. 373, 287–311.

Batchelor, G., Proudman, I., 1954. The effect of rapid distortion of a fluid in turbulent motion. Q. J. Mech. Appl. Math. 7, 83–103.

Bernstein, O., Shapiro, M.J., 1994. Direct determination of the orientation distribution function of cylindrical particles immersed in laminar and turbulent flow. J. Aerosol. Sci. 25, 113–136.

Bibbo, M.A., Dinh, S.M., Armstrong, R.C., 1985. Shear flow properties of semiconcentrated fiber suspensions. J. Rheology 29, 905–929.

Brenner, H., 1974. Rheology of a dilute suspension of axisymmetric Brownian particles. Int. J. Multiphase Flow 1, 195–241.

Brown, M.L., Parsheh, M., Aidun, C.K., 2006. Turbulent flow in a converging channel: effect of contraction and return to isotropy. J. Fluid Mech. 560, 437–448.

Comte-Bellot, G., Corrsin, S., 1966. The use of a contraction to improve the isotropy of grid-generated turbulence. J. Fluid Mech. 25, 657–682.

Ding, E.J., Aidun, C.K., 2000. The dynamics and scaling law for particles suspended in shear flow with inertia. J. Fluid Mech. 423, 317–344.

Dinh, S.M., Armstrong, R., 1984. A rheological equation of state for semiconcentrated fiber suspensions. J. Rheology 28, 207–227.

Doi, M., Edwards, S.F., 1988. Theory of Polymer Dynamics. Oxford University Press, England.

Goldsmith, H.L., Mason, S.G., 1967. The microrheology of dispersions. In: Eirich, F.R. (Ed.), Rheology: Theory and Applications, vol. IV. Oxford University Press, Academic.

Hussain, A., Ramjee, V., 1976. Effects of the axisymmetric contraction shape on incompressible turbulent flow. J. Fluids Eng. 98, 897.

Jeffery, G., 1922. The motion of ellipsoidal particles immersed in viscous fluid. Proc. R. Soc. Lond. A 102, 161–179.

Koch, D.L., 1995. A model for orientational diffusion in fiber suspensions. Phys. Fluids 7, 2086–2088.
Krushkal, E., Gallily, I., 1988. On the orientation distribution function of non-spherical aerosol particles in a general shear flow. J. Aerosol Sci. 19, 197–211.
Olson, J.A., 2002. Analytic estimate of the fibre orientation distribution in a headbox flow. Nordic Pulp Paper J. 17, 302–306.
Olson, J.A., Kerekes, R.J., 1998. The motion of fibres in turbulent flow. J. Fluid Mech. 377, 47–64.
Olson, J.A., Frigaard, I., Candice, C., Hämaläinen, J.P., 2004. Modelling a turbulent fibre suspension flowing in a planar contraction: the one-dimensional headbox. Int. J. Multiphase Flow 30, 51–66.
Parsheh, M., Brown, M.L., Aidun, C.K., 2005. On the orientation of stiff fibres suspended in turbulent flow in a planar contraction. J. Fluid Mech. 545, 245–269.
Paschkewitz, J.S., Dimitropoulos, C.D., Hou, Y.X., Somandepalli, V.S.R., Mungal, M.G., Shaqfeh, E.S.G., Moin, P., 2005. An experimental and numerical investigation of drag reduction in a turbulent boundary layer using rigid rodlike polymers. Phys. Fluids 17, 085101-1–085101-16.
Ramjee, V., Hussain, A., 1976. Influence of axisymmetric contraction on free-stream turbulence. J. Fluids Eng. 98, 506–515.
Ribner, H., Tucker, M., 1953. Spectrum of turbulence in a contracting stream. NACA Rept., 1113.
Shaqfeh, E.S.G., 1988. A nonlocal theory for the heat transport in composites containing highly conducting fibrous inclusions. Phys. Fluids 31, 2405–2425.
Shaqfeh, E.S.G., Fredrickson, G.H., 1990. The hydrodynamic stress in a suspension of rods. Phys. Fluids A 2, 7–24.
Shaqfeh, E.S.G., Koch, D.L., 1990. Orientation dispersion of fibres in extensional flows. Phys. Fluids A 2, 1077–1093.
Shin, M., Koch, D.L., 2005. Rotational and translational dispersion of fibers in isotriopic turbulent flows. J. Fluid Mech. 540, 143–173.